Journal of Inclusion Phenomena and Molecular Recognition in Chemistry **13**: 207–218, 1992.

Synthesis and Characterization of Gallosilicate Pentasil (MFI) Framework Zeolites*

S. V. AWATE, P. N. JOSHI, V. P. SHIRALKAR and A. N. KOTASTHANE
National Chemical Laboratory, Pune 411008, India

(Received: 11 July 1990; in final form: 8 April 1992)

Abstract. Crystalline gallosilicates with a pentasil (MFI) framework containing Ga^{3+} in lattice positions were synthesised. The kinetic features of the hydrothermal system containing triethyl-*n*-butylammonium cations $(TEBA)^+$ as template in the gel system

$$Na_2O : (TEBA)_2O : Ga_2O_3 : SiO_2 : H_2O$$

have been investigated. The gallosilicate products were characterized by XRD, framework-IR, TG/DTA, ^{29}Si and ^{71}Ga MASNMR and sorption measurements using standard techniques.

The values of the apparent activation energies for nucleation (E_n) and crystallization (E_c) were evaluated by applying the Arrhenius equation. Evidence from ^{29}Si and ^{71}Ga MASNMR as well as the estimated unit-cell volumes computed from XRD powder patterns indicate that a significant amount of Ga^{3+} is substituted in the pentasil (MFI) framework.

Key words. Gallosilicate (MFI) synthesis, crystallization kinetics, ^{29}Si ^{71}Ga MASNMR, XRD, IR.

1. Introduction

Tectosilicate framework zeolites can be modified by the substitution of the Si or Al atoms [1]. Such modifications are often referred to in the literature as 'isomorphous or heteroatom substitutions' during zeolite synthesis [2]. An isomorphous substitution with tetravalent or trivalent elements, for example B/Fe/Ga/Cr/La/Ti/Ge etc., replacing Al^{3+} or Si^{4+} has aroused widespread interest. It is expected that such replacements would greatly modify the nature and strength of the acid sites in the zeolites.

A number of studies on various framework gallosilicates including ABW [3], FAU [4], LTL [5], MAZ [6], NAT and SOD [7] have been reported. In addition, the gallium analog of ZSM-5 has been described in the seventies [8] and more recently by many authors [9–11]. The chemical properties of gallium are similar to those of aluminium, but the ionic radius of the Ga ion (0.62 Å) is greater than that of the Al ion (0.51 Å). Considering these aspects, the expected difference in the metal–oxygen bond length (Ga—O 1.82 Å, Si—O 1.61 Å, Al—O 1.75 Å) would control the pore structure and thus either increase or decrease the unit cell volume. It is of interest to examine the manner in which isomorphous substitution by Ga ions influences the crystallization kinetics for pentasil framework zeolites. In this paper we report the salient features of the hydrothermal synthesis of gallium analogs of pentasil framework zeolites. The crystallization kinetics have been examined systematically.

* N.C.L. Communication No. 4951.

2. Experimental

2.1. MATERIALS AND ZEOLITE SYNTHESIS

Reactants used for the synthesis of MFI framework gallosilicates were aqueous sodium silicate (28.0% SiO_2, 8.4% Na_2O), gallium sulfate (>98%, AG Aldrich), H_2SO_4 (98% BDH), triethyl-*n*-butylammonium bromide (TEBA-Br) and deionized water. The detailed procedure followed to prepare a reactive hydrogel was similar to the one developed previously [12]. A reactive synthetic gallosilicate gel having the oxide mole composition

$$4.4\,(TEBA)_2O : 24.1\,Na_2O : Ga_2O_3 : 85.0\,SiO_2 : 3275\,H_2O$$

was transferred into a stainless steel autoclave and crystallized at 473, 453 and 433 K, in static conditions, under autogenous pressure for various lengths of time (1–70 h). After the crystallization, the solid products were filtered, washed with deionized water and dried at 398 K overnight.

2.2. ANALYSIS AND CHARACTERIZATION

The gallosilicate products were identified by X-ray diffraction (XRD) using a Philips PW 1730 diffractometer with Ni-filtered CuK_α radiation in 2θ range 5–50°. The percent crystallinity of gallosilicate was also estimated using a previously reported [13] relation. For the highly crystalline samples pure Si was used as an internal standard during XRD studies for estimating unit cell volumes. The chemical composition of the as-synthesised gallosilicate products was established by wet-chemical methods using atomic absorption (Hitachi-8000) and inductively coupled plasma (Jobin Yvon, France) spectrophotometers. ^{29}Si and ^{71}Ga magic-angle spinning (MASNMR) spectra were recorded at 59.6 MHz and 91.5 MHz, respectively, with a Bruker MSL-300 NMR spectrometer at ambient temperature. The spinning rate of the rotor containing the gallosilicate sample was kept between 3.0 to 3.2 KHz. Chemical shifts are referred to hexamethyl disiloxane, 6.7 ppm from TMS, with high field shifts being negative. Thermoanalytical measurements were made on a Netzsch model STA 490 in the temperature range 298–1273 K. The heating rate was 10 K min^{-1}, the air flow was 3.4 $dm^3\,h^{-1}$ and the amount of sample was 50 mg. Framework infrared (IR) spectra of the lattice vibrations for gallosilicates were recorded with a Pye Unicam SP-300 spectrometer using the KBr pellet technique. Sorption measurements were conducted using an all glass McBain type (balance) gravimetric unit at 298 K and $P/P_0 = 0.8$.

3. Results and Discussion

A list of samples investigated is reported in Table I together with data concerning the chemical composition of both the reaction mixture and the crystallized gallosilicate products. The gallium content was controlled by varying the composition of the reaction mixture.

Inspection of the XRD powder pattern (Figure 1) clearly indicates that the Ga analog possesses a pentasil (MFI) framework structure with traces of amorphous impurities. However, most of the reflections in the XRD pattern show a slight shift

Table I. Composition of hydrogel, product and unit cell volume for gallosilicate pentasil zeolites

Sample	Hydrogel composition			Product analysis		Unit cell volume (V Å^3)
	SiO_2	Na_2O	OH^-	SiO_2	Na_2O	
	Ga_2O_3	Ga_2O_3	H_2O	Ga_2O_3	Ga_2O_3	
I	40	11.1	0.55×10^{-3}	39	0.75	5402
II	85	24.1	2.72×10^{-3}	77	0.74	5389
III	400	82.1	4.03×10^{-3}	341	0.68	5351
Silicalite	>2000	–	–	1185	0.58	5280

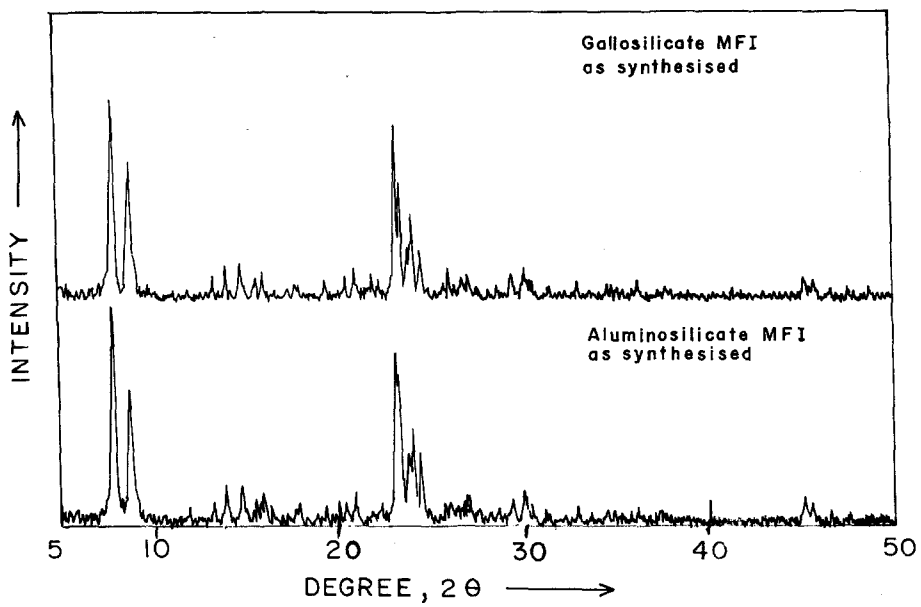

Fig. 1. X-ray powder diffraction patterns of aluminium and gallium containing pentasil (MFI) framework structures.

in the interplanar spacings (d Å) towards higher values in comparison with that of the Al analog. The observed lattice expansion may be a consequence of the incorporation of larger gallium ions in place of aluminium into the silicate framework during the synthesis. The fact that insertion of gallium ions in the faujasite framework causes an unit-cell expansion was reported by Kuhl in the early 1970s [4]. The results on estimated unit cell volumes are shown in Figure 2 along with those of the Al analog samples for comparison. It can be seen that the unit cell volume expands linearly with decreasing SiO_2/Ga_2O_3 ratio indicating successful insertion of larger Ga ions during the hydrothermal synthesis. Simmons *et al.* [11] also observed a similar trend while confirming Ga framework incorporation.

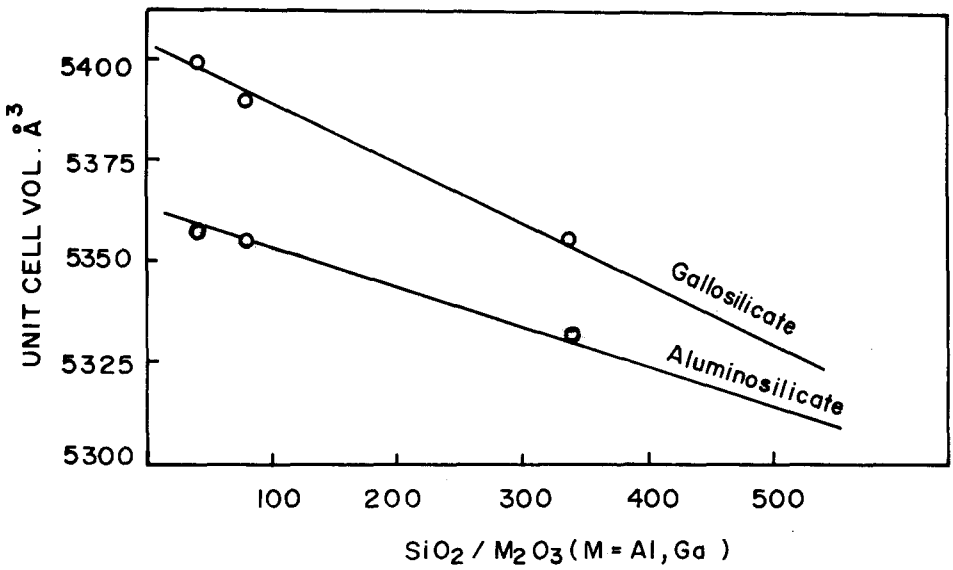

Fig. 2. Relationship between unit cell volumes of alumino and gallosilicates.

3.1. KINETICS OF CRYSTALLIZATION

The crystallization curves in the temperature range 433–473 K for gallosilicate using triethyl-*n*-butylammonium bromide (TEBA-Br) as a templating species are shown in Figure 3. The reaction mixture which was defined by the following molar ratios $SiO_2/Ga_2O_3 = 85$, $Na_2O/Ga_2O_3 = 24.1$ and $OH^-/H_2O = 2.72 \times 10^{-3}$ was adopted to study the effect of temperature on the formation of gallosilicate zeolite. The crystallinity of gallosilicate phases varied with the crystallization time according to the classical sigmoidal growth curves usually observed in non-seeded systems [1]. Apparently, the solubility of the gallosilicate gel was enhanced on increasing the crystallization temperature. However, with longer crystallization times (usually after attaining 100% crystallinity), a decrease in crystallinity (not shown in Figure 3) was observed due to the formation of a dense phase impurity (like α-quartz) at the expense of the crystalline pentasil phase. Hence, the metastability region for gallosilicate pentasil zeolite is found to be smaller in the present studies compared to that for the aluminosilicate pentasil zeolite. It was also shown [12, 14] that the processes of pentasil zeolite nucleation and successive crystal growth could be represented mathematically by the Avarami–Erofeev equation

$$\ln[1/(1-\alpha)] = (kt)^m \tag{1}$$

where α and t are fractional conversion and time, respectively, and k and m are constants. The data in Figure 3 were fitted to Equation (1) and the values of k and m obtained from linear plots are compared and tabulated in Table II. The increase in k values and decrease in m values with the rise in synthesis temperature corresponds to the general expectations in consideration of the temperature dependent nucleation and crystallization processes. A good fit of the data (correlation coefficient ~ 1, Table II) indicates that the gallosilicate pentasil formation can be

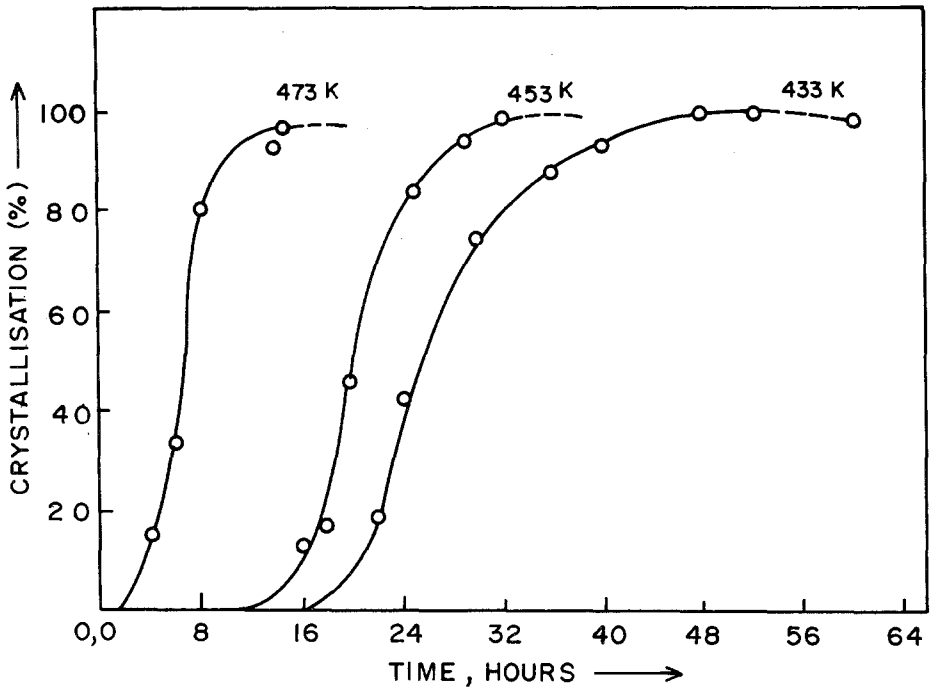

Fig. 3. Crystallization kinetics of gallium analog of pentasil (MFI) framework zeolites.

Table II. Avarami–Erofeev parameters for gallosilicate synthesis using TEBA-Br

Synthesis temp. K	$10^2 \times k$	m	Correlation coefficient
433	3.27	4.72	0.99
453	4.58	3.60	0.98
473	11.73	2.44	1.03

successfully described, at least mathematically, by the Avarami–Erofeev equation. Considering the formation of the nuclei during the induction period as an energetically activated process and that nucleation is the rate determining step during the induction period, the apparent activation energy for nucleation E_n was estimated by applying the relationship:

$$\mathrm{d}\ln(1/\theta)/\mathrm{d}(1/T) = -E_n/RT \tag{2}$$

to the temperature dependence of the rate of nucleation where θ is the induction period, i.e. the point on the crystallization curve where conversion to the crystalline phase is just starting. T is the absolute temperature and R is the gas constant. The rate of nucleation was assumed to be inversely proportional to the induction period. Similarly E_c, the apparent activation energy for crystal growth, was calculated from

the temperature dependence of the rate of crystallization, assuming that the rate of crystallization was obtained from the inflection point in the crystallization curve (i.e. at the highest rate of crystallization).

$$\mathrm{d}\ln K/\mathrm{d}(1/T) = -E_c/RT \tag{3}$$

In Equation (3) K is the point on the crystallization curve where 50% crystallization is complete; T and R have their usual meanings.

The linear plots obtained by applying the more useful form of the Arrhenius Equations (2) and (3) are shown in Figure 4. The values of the apparent activation energy of nucleation ($E_n = 155.7$ kJ mol^{-1}) as well as that of crystallization ($E_c = 94.3$ kJ mol^{-1}) for the gallosilicate analog of pentasil formation were evaluated from the slopes of these linear plots. The above values of E_n and E_c obtained during the present studies appear to be higher than those reported previously [12] for the Al analog ($E_n = 118$, $E_c = 78.6$ kJ mol^{-1}) and the Fe analog [15] ($E_n = 145$, $E_c = 92.5$ kJ mol^{-1}) pentasil zeolites. However, the corresponding E_n and E_c values increase in the order ($Al^{3+} \rightarrow Fe^{3+} \rightarrow Ga^{3+}$) of increasing ionic radii. It is considered that the nucleation rate depends on the nature of the metal cationic species and their ability to condense with the silicate species. The condensation ability gradually weakens in the odder (Al → Fe → Ga) with increasing ionic radius. Based on this, the

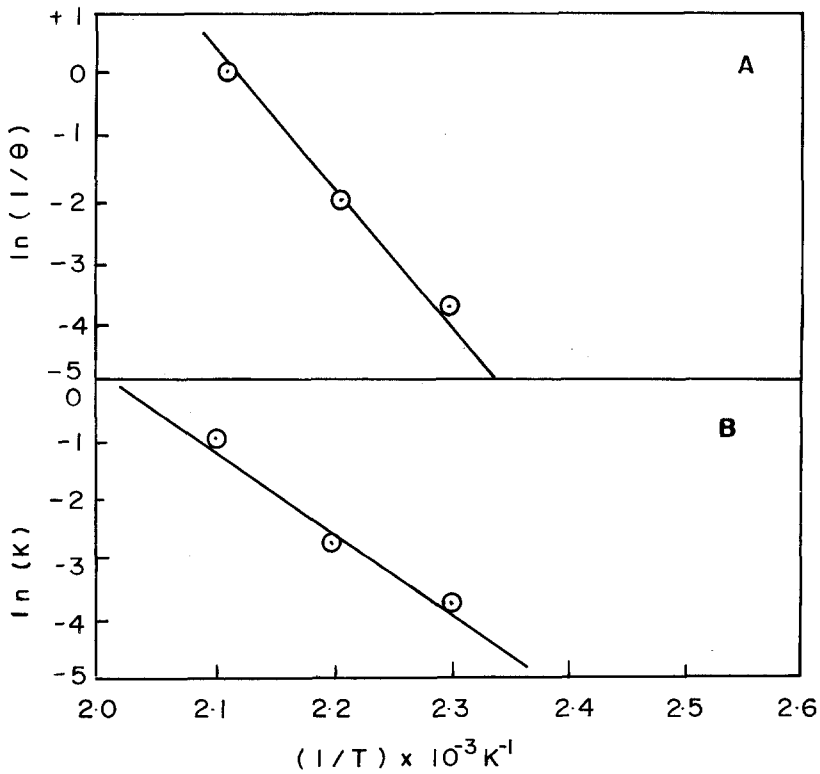

Fig. 4. Arrhenius plots for (A) nucleation and (B) crystallization of gallium analog of MFI type zeolites.

weakening of condensation correlates well with the increased E_n value for the gallosilicate pentasil of this work. Similarly, the experimental results for the crystal growth in terms of apparent activation energy of crystallization showed an increasing trend from $Al^{3+} \rightarrow Ga^{3+}$, which is also consistent with the lower gel dissolution rate during the crystal formation in the order of increasing ionic radius from $Al^{3+} \rightarrow Ga^{3+}$.

To delineate the behavior of gallium during crystallization, the bulk chemical composition of the intermediate phases, obtained by AAS and ICP techniques and expressed as Si/Ga and Ga/Na atomic ratios, are presented in Figure 5. Initially (up to 15 h) the Si/Ga ratio is high, and remains constant, suggesting that gallosilicate crystallites essentially involve a silica rich core. Subsequently the Si/Ga ratio decreases, indicating progressive incorporation of Ga into the framework. This suggests that liquid phase transportation may be operative during the formation of gallosilicate zeolite. This is consistent with the observation reported previously for the Al–ZSM-5 system [16]. In addition, the Ga/Na atomic ratio is initially low but

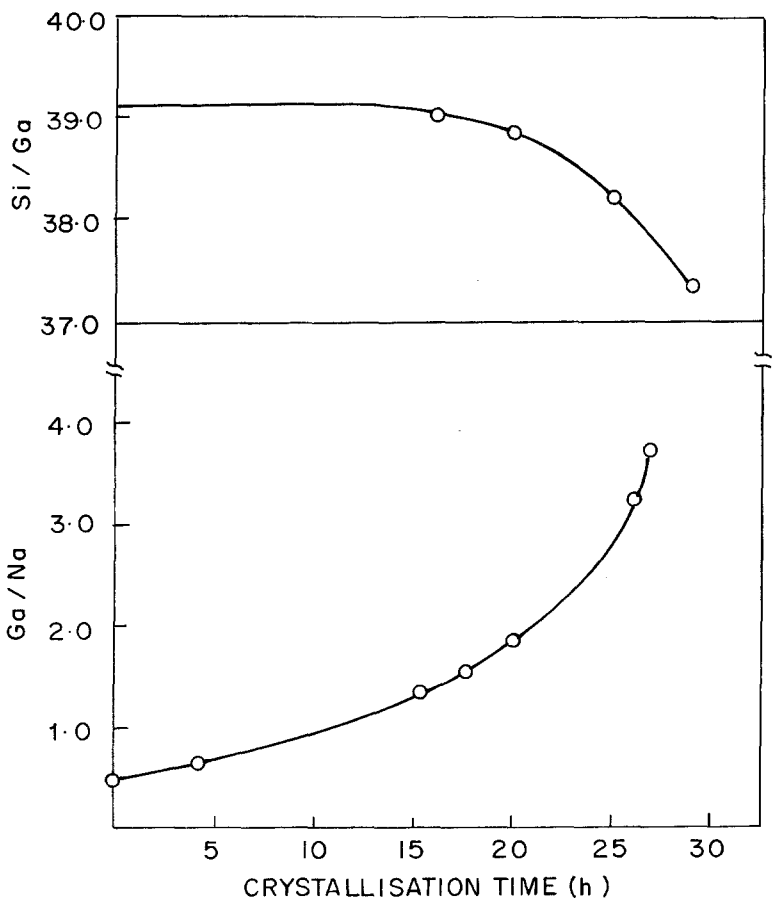

Fig. 5. Variation of Si/Ga and Ga/Na atomic ratios of the intermediate solid phases formed during crystallization of MFI type zeolites (Sample II, Table I).

rapidly increases (ca. Ga/Na = 4) indicating that Na^+ are compensating for about 25% of the Ga present. However, it indicates that the amount of Na^+ ions occluded into the gallosilicate is lower than the number of negative charges present in the framework. It is more likely that the $TEBA^+$ ions incorporated during the synthesis may be acting as charge compensating cations on GaO_4 tetrahedra and thus contributing to the neutralization of the gallosilicate zeolitic lattice. This is also consistent with findings from the synthesis of Al–ZSM-5.

3.2. FRAMEWORK IR

Figure 6 shows framework region IR spectra of the gallosilicate products along with the silicalite sample. In the case of gallosilicate samples 1, 2 and 3, with SiO_2/Ga_2O_3 ratios of 39, 77 and 341 respectively, the asymmetric stretching bands ($1100\ cm^{-1}$) are found to shift to lower wavenumbers with respect to silicalite (sample 5) and a gallium impregnated ($\sim$4–5 wt.-%) silicalite sample (sample 4). This is due to the change occurring in the force constant of the T—O bond by the

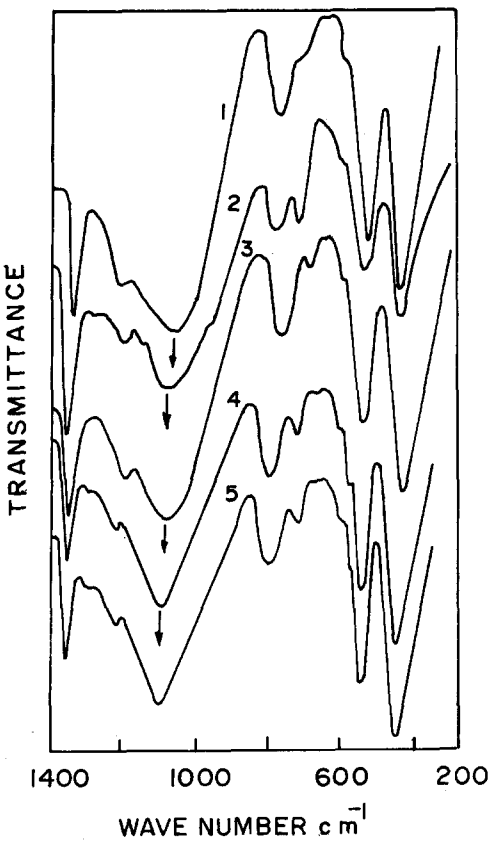

Fig. 6. I.R. spectra of: (1) gallosilicate ($R = 39$); (2) gallosilicate ($R = 77$); (3) gallosilicate ($R = 341$); (4) Ga-impregnated silicalite; and (5) pure silicalite.

insertion of the comparatively heavier gallium into the framework. The shift of the asymmetric stretching frequency is also known for Fe and P substitution into the zeolitic frameworks [13, 17].

3.3. SORPTION MEASUREMENTS

Table III lists the selected sorption data for the gallosilicate along with the silicalite and impregnated silicalite samples. Water sorption consistently decreases with a decrease of gallium in the zeolite. This suggests an increase in the hydrophillic character of the gallosilicate with the decreased SiO_2/Ga_2O_3 ratios. On the other hand, the nearly constant equilibrium sorption of *n*-hexane corresponds to generally observed and reported trends for zeolite ZSM-5 [18, 19]. The equilibrium sorption capacities for almost nonpolar sorbate molecules like *n*-hexane were found to be unaffected by the variation of the gallium content in the gallosilicate pentasil samples. However, relatively higher values for water and cyclohexane adsorption on gallosilicate, compared to those for silicalite and impregnated samples, further indicate some change in the void volume when Ga^{3+} is present and occupying tetrahedral positions in the lattice. This further supports the conclusion that under direct hydrothermal treatment Ga containing hydrogels yield a Ga^{3+} containing zeolite framework, and do not produce silicalite with occluded Ga_2O_3.

3.4. THERMAL ANALYSIS

Figure 7 shows TG/DTA curves for 100% as-synthesized gallosilicate sample II (Table I). Three distinct zones of weight loss can be distinguished in the following temperature ranges: (I) 434–550 K; (II) 647–699 K; and (III) 699–834 K. The first step results from dehydration of physically sorbed water. The other two steps are exothermic (DTA curve) and are related to the oxidative decomposition of organic material. This is consistent with the characteristic two step exotherms usually found in the Al analog of MFI framework zeolites [20]. The low temperature (705 K) peak is believed to be due to decomposition of loosely held $TEBA^+$ ions in gallosilicate, while the high temperature (757 K) peak corresponds to the oxidative decomposition of $TEBA^+$ cations which are strongly bonded and associated with

Table III. Sorption properties of gallosilicate

	Sorption, gm. 100 gm^{-1}*		
SiO_2/Ga_2O_3	*n*-C_6H_{14}	H_2O	C_6H_{12}
Gallosilicate, $R = 39$	10.1	9.1	5.9
Gallosilicate, $R = 77$	11.0	8.1	4.5
Gallosilicate, $R = 341$	11.5	4.0	4.0
Silicalite, $R = 1185$	11.9	3.3	3.6
Ga-impregnated silicalite	12.1	3.3	3.5

* At 298 K, $P/P_0 = 0.8$.

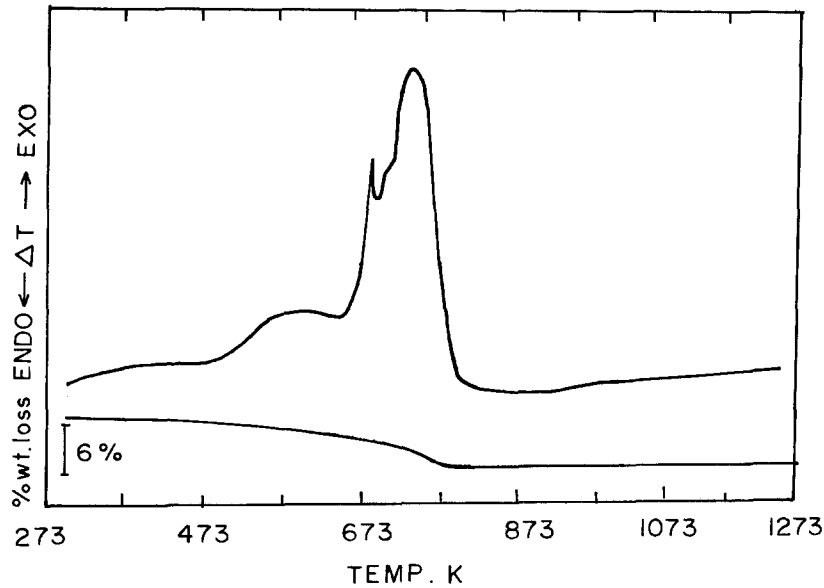

Fig. 7. TG/DTA curves for 100% crystalline as-synthesized gallosilicate.

gallium acid sites in the channels. There are no significant thermal effects between 834–1273 K, indicating the essentially high thermal stability of gallosilicate pentasil samples of this study.

3.5. ^{29}Si AND ^{71}Ga MASNMR

The ^{71}Ga MASNMR spectrum of as-synthesized gallosilicate analog samples is shown in Figure 8. For comparison the ^{71}Ga MASNMR spectrum of gallium sulfate (in which gallium is known to have an octahedral coordination [21]) is also shown. The chemical shift $\delta = -87$ ppm for gallium atoms in solid $Ga_2(SO_4)_3$ is characteristic of Ga in octahedral sites. The ^{71}Ga MASNMR spectrum for as-synthesized gallosilicate analog containing gallium showed a large chemical shift at $\delta = 163$ ppm for Ga^{3+}. Thus the position of the $\delta = 163$ ppm peak is attributed to Ga^{3+} ions in tetrahedral environments with respect to oxygen in the gallosilicate analog of pentasil zeolite framework [22, 23].

A study using ^{29}Si MASNMR (Figure 8) of three different samples: (a) pure silicate; (b) gallosilicate with SiO_2/Ga_2O_3 of 341; and (c) gallosilicate with SiO_2/Ga_2O_3 of 39, showed two types of Si ordering in the as-synthesized gallosilicate. The chemical shift value of about -103 ppm, corresponds to Si(1T) environments and a large signal at about -112 ppm corresponds to Si(0T) atoms. Hence, the signal at $\delta = -103$ ppm can be attributed to Si atoms having Ga atoms in their second coordination sphere. The peaks marked with an asterisk (*) are due to the spinning side-bands. The apparent line intensity changes were found to be consistent [21] with the Ga content (SiO_2/Ga_2O_3) of these gallosilicates.

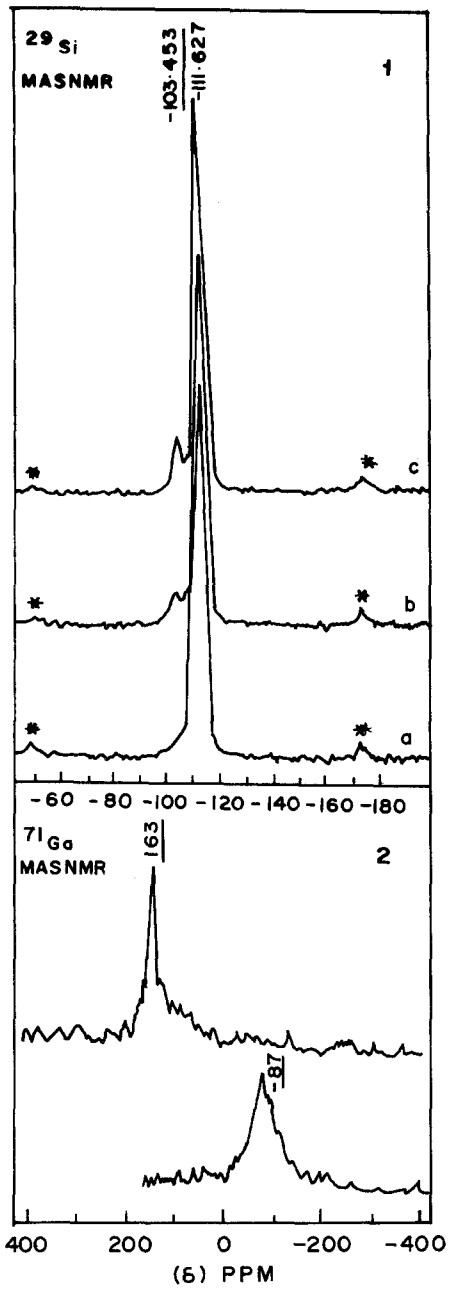

Fig. 8. (1) ^{29}Si MASNMR spectra of samples (a) silicalite, (b) gallosilicate ($R = 341$) and (c) gallosilicate ($R = 39$). The shifts are given relative to TMS. (2) ^{71}Ga MASNMR spectra of as-synthesized gallosilicate MFI zeolite indicating the tetrahedral environment of Ga (163 ppm) and the octahedral coordination of Ga within $Ga_2(SO_4)_3$ (-87 ppm). The chemical shifts are given relative to $Ga(H_2O)_6^{3+}$ in aqueous solution.

4. Conclusions

A gallosilicate derivative of the pentasil framework (MFI) has been prepared following a route of primary hydrothermal synthesis. X-ray diffraction analysis of as-synthesised gallosilicate zeolite with MFI framework reveals structural characteristics similar to analogous MFI framework aluminosilicates. The manner in which the framework adjusts to accommodate Ga^{3+} incorporation is demonstrated by the observed increase in unit-cell volumes. Evidence from framework IR and high resolution ^{29}Si and ^{71}Ga MASNMR further supports the conclusion of Ga^{3+} insertion into the silicate framework.

References

1. R. M. Barrer: *Hydrothermal Chemistry of Zeolites*, Academic Press, London, Ch. 6 (1982).
2. T. Tielen, M. Geelen and P. A. Jacobs: *Acta Phys. Chem.* **31**, 1 (1985).
3. J. M. Newsam and D. E. W. Vaughan: in *New Developments in Zeolite Science Technology*, eds. Y. Murakami, A. Lijima and J. W. Ward, Kodansha, Tokyo, Japan (1986), pp. 457–464.
4. G. B. Kuhl: *J. Inorg. Nucl. Chem.* **33**, 3261 (1971).
5. P. A. Wright, J. M. Thomas, A. K. Cheetham and A. Nowak: *Nature* **318**, 611 (1985).
6. J. M. Newsam, R. H. Jarman and A. J. Jacobson: *Mater. Res. Bull.* **20**, 125 (1985).
7. D. Xie, J. M. Newsam, J. Yang and B. Yelon: *Mater. Res. Soc., Symp., Proc.* Vol. III (1988), p. 147.
8. H. W. Kouwenhoven, W. H. J. Stork and L. Schaper: *Offenheg. Schritt* 2755770 (1978).
9. Xu Ruren and Pang Wenqin: *Stud. Surf. Sci. Catal.* **24**, 27 (1985).
10. G. P. Handreck and T. D. Smith: *J. Chem. Soc., Faraday Trans., I.* **85**, 3215 (1989).
11. D. K. Simmons, R. Szostak and P. K. Agrawal: *J. Catal.* **106**, 287 (1987).
12. P. N. Joshi, G. N. Rao, A. N. Kotasthane and V. P. Shiralkar: *J. Incl. Phenom.* **9**, 91 (1990).
13. S. B. Kulkarni, V. P. Shiralkar, A. N. Kotasthane, R. B. Borade and P. Ratnasamy: *Zeolites* **2**, 313 (1982).
14. V. P. Shiralkar and A. Clearfield: *Zeolites* **9**, 363 (1989).
15. A. N. Kotasthane: Ph.D. Thesis, University of Pune (1985).
16. E. G. Derouane, S. Detremmerie, Z. Gabelica and N. Blom: *Appl. Catal.* **1**, 201 (1981).
17. E. M. Flanigen and R. M. Grose: *Adv. Chem. Ser.* **101**, 76 (1971).
18. J. R. Anderson, K. Foger, T. Mole, R. A. Rajadhyaksha and J. V. Senders: *J. Catal.* **58**, 114 (1979).
19. H. J. Doelle, J. Hearing, L. Riekert and L. Marosi: *J. Catal.* **71**, 27 (1981).
20. A. N. Kotasthane and V. P. Shiralkar: *Thermochim. Acta* **102**, 3 (1986).
21. V. M. Mastikhin and K. I. Zamaraev: *Z. Phys. Chem. Neue Folge* **152**, 59 (1987).
22. J. W. Akitt: *Annu. Rep. NMR Spectroscopy* **5A**, 465 (1972).
23. J. M. Thomas, J. Klinowsky, S. Ramadas, M. W. Anderson, C. A. Fye and G. C. Gobbi: *Intrazeolite Chemistry*, ACS Symp. Series, ACS Washington DC, Vol. 218 (1983), p. 159.